Photostability of dye molecules trapped in solid matrices

Arnaud Dubois, Michael Canva, Alain Brun, Frédéric Chaput, Jean-Pierre Boilot

Photostability of dye molecules trapped in solid matrices

Arnaud Dubois, Michael Canva, Alain Brun, Frédéric Chaput, and Jean-Pierre Boilot

The photostability of dye molecules trapped in transparent solid matrices synthesized by the solgel technique was studied both experimentally and theoretically using a model with numerical and approximate analytical solutions. The model is based on a one-photon photodestruction process with the creation of an absorbing bleached molecule. We give the number of photons that different trapped dye molecules can absorb on average before they are bleached. Dyes such as Perylene Red, Perylene Orange, Pyrromethenes 567 and 597, Rhodamines 6G and B, DCM, a Xanthylium salt, and Neon Red were investigated; significant differences were observed. Some dye molecules in solvents were also studied; increased stability resulted when the molecules were trapped in solid matrices.

Key words: Photostability, dye molecules, solgel process.

1. Introduction

Organic dye molecules have been used for many years in both lasers and optically pumped amplifiers. Dye lasers offer attractive qualities such as high quantum efficiency, a large choice of pump source, and a broad emission bandwidth. They are of continuing interest because of their capacity, with different dyes, to cover the spectrum from the ultraviolet to the infrared. Dyes are used to get continuous or pulsed emissions from the femtosecond to the microsecond range. Compared with other laser sources, they are often less expensive. Unfortunately dye molecules are used in solvents that require large reservoirs along with circulation apparatus in order to supply fresh molecules permanently to the active region. Because of their limited lifetime, dye solutions have to be replaced quite often, which requires significant maintenance and produces toxic waste.

Much research has been done to trap dye molecules in solid matrices with appropriate thermal, chemical, mechanical, and optical properties. Efficient solid-state dye lasers were recently obtained using matrices prepared by the solgel process[1–4] or with polymeric matrices.[5] The photostability of some organic laser dyes improves when molecules are trapped in solid matrices.[6–9] Nevertheless, because of the absence of dye reservoirs and circulation systems in solid-state dye lasers, photostability is a critical issue.

The purpose of our research was to study both experimentally and theoretically the photostability of different dye laser molecules trapped in solid matrices synthesized by the solgel technique. We also want to estimate the stability increase of dye molecules in solid matrices compared with molecules in liquid solutions. We present a theoretical model of photodestruction of dye molecules when illuminated with a continuous laser light. This model involves a one-photon process in which the dye molecules are progressively transformed into stable bleached molecules with weak absorbance. An important part of the experimental study was to check that other destructive processes not taken into account in the model were negligible in our working conditions. Then we matched our experimental results to the model and obtained for each of our dye molecules a physical parameter of photostability: the average number B of photons that they can absorb before bleaching.

2. Theoretical Model of Photodestruction

It is well known that organic dye molecules are progressively bleached when they are illuminated in

A. Dubois, M. Canva, and A. Brun are with the Institut d'Optique Théorique et Appliquée, Unité associée 14, Centre National de la Recherche Scientifique, Bâtiment 503, B. P. 147, 91403 Orsay Cedex, France. F. Chaput and J.-P. Boilot are with the Groupe de Chimie du Solide, Laboratoire de Physique de la Matière Condensée, Unité de Recherche Associée 1254 D, Centre National de la Recherche Scientifique, Ecole Polytechnique, 91128 Palaiseau Cedex, France.

Received 19 September 1995; revised manuscript received 23 January 1996.

0003-6935/96/183193-07$10.00/0

their absorption band; they are transformed into components that have much lower absorption in this band.[9–14] Different physical mechanisms are possible. We present a simple theoretical model based on a one-photon process in which each dye molecule has a certain probability of being transformed into a bleached molecule after having absorbed a certain number of photons. We assume a uniform distribution of isotropic dye molecules. The bleached molecules progressively created during illumination are assumed to be stable, although slightly absorbing.

A. Analytical Solution

When exposure starts at $t = 0$ only the dye molecules (species 1) are present, uniformly distributed with a volumetric concentration N_0. We assume the continuous light to be incident in the z direction with $z = 0$ corresponding to the input face of the sample of thickness L. We neglect the propagation time of the light in the sample. During exposure the incident light progressively converts the dye molecules into bleached molecules (species 2). Denoting the densities of the two species by $N_1(z, t)$ and $N_2(z, t)$, respectively, our first relation is

$$N_1(z, t) + N_2(z, t) = N_0. \tag{1}$$

The number of molecules per unit area in length z are for the two species:

$$J_1(z, t) = \int_0^z N_1(z', t)\mathrm{d}z',$$

$$J_2(z, t) = \int_0^z N_2(z', t)\mathrm{d}z', \tag{2}$$

from which we have the relationship

$$J_1(z, t) + J_2(z, t) = N_0 z. \tag{3}$$

Setting $z = L$ in Eq. (3) yields

$$J_1(L, t) + J_2(L, t) = N_0 L = J_0. \tag{4}$$

The local flux of photons with wavelength λ can be written as follows:

$$n(z, t) = n_0 \exp[-\sigma_1 J_1(z, t) - \sigma_2 J_2(z, t)], \tag{5}$$

where n_0 is the incident flux of photons and σ_1, σ_2 are the absorption cross sections for the two species. Using Eq. (3), the local flux of photons can be rewritten as

$$n(z, t) = n_0 \exp[-\Delta\sigma J_1(z, t)]\exp(-\sigma_2 N_0 z), \tag{6}$$

where $\Delta\sigma = \sigma_1 - \sigma_2$.

We define bleaching number B as the average number of photons absorbed by a dye molecule before it is bleached (B^{-1} is the quantum efficiency for bleaching). The local bleaching rate is

$$\frac{\partial N_1(z, t)}{\partial t} = -\sigma_1 N_1(z, t) B^{-1} n(z, t). \tag{7}$$

Integrating both sides of Eq. (7) over thickness L yields the total bleaching rate:

$$\frac{\mathrm{d}J_1(L, t)}{\mathrm{d}t} = \int_0^L -\sigma_1 N_1(z, t) B^{-1} n(z, t)\mathrm{d}z. \tag{8}$$

Using Eq. (6) we obtain

$$\frac{\mathrm{d}J_1(L, t)}{\mathrm{d}t} = -\sigma_1 B^{-1} n_0 \int_0^L N_1(z, t) \times \exp[-\Delta\sigma J_1(z, t)]\exp(-\sigma_2 N_0 z)\mathrm{d}z, \tag{9}$$

and with Eq. (2) we obtain

$$\frac{\mathrm{d}J_1(L, t)}{\mathrm{d}t} = \frac{\sigma_1 B^{-1} n_0}{\Delta\sigma} \int_0^L \frac{\partial}{\partial z}[-\Delta\sigma J_1(z, t)] \times \exp[-\Delta\sigma J_1(z, t)]\exp(-\sigma_2 N_0 z)\mathrm{d}z. \tag{10}$$

Differential Eq. (10) cannot be solved analytically. However, with the approximation $\exp(-\sigma_2 N_0 z) = 1$, we are able to give an analytical solution. This approximation is possible if $\sigma_2 N_0 z \ll 1$ when $0 \le z \le L$. Therefore, the condition for the validity of the approximation is $\sigma_2 N_0 L \ll 1$. Then Eq. (10) becomes

$$\frac{\mathrm{d}J_1(L, t)}{\mathrm{d}t} = \frac{\sigma_1 B^{-1} n_0}{\Delta\sigma}[\exp[-\Delta\sigma J_1(L, t)] - 1]. \tag{11}$$

Equation (11) can be rewritten as

$$\frac{\mathrm{d}x}{x(1 - x)} = \sigma_1 B^{-1} n_0 \mathrm{d}t \tag{12}$$

where $x = \exp[-\Delta\sigma J_1(L, t)]$. The integration gives

$$\ln\left(\frac{x}{1 - x}\right) = \sigma_1 B^{-1} n_0 t + \text{const}. \tag{13}$$

With the initial condition $J_1(L, 0) = J_0$ we finally obtain

$$\exp[-\Delta\sigma J_1(L, t)] = \frac{1}{1 + \exp(\Delta\sigma J_0 - 1)\exp(-\sigma_1 B^{-1} n_0 t)}. \tag{14}$$

Hence the evolution of the number of dye molecules per unit area (normalized) is

$$\frac{J_1(L, t)}{J_1(L, 0)} = \frac{\ln[1 + \exp(\Delta\sigma J_0 - 1)\exp(-\sigma_1 B^{-1} n_0 t)]}{\ln[1 + \exp(\Delta\sigma J_0 - 1)]}. \tag{15}$$

This can be simply written as a function of the integrated input energy per unit area E

($E = n_0 \times h \times v \times t$, where h is Planck's constant):

$$\frac{J_1(L, E)}{J_1(L, 0)} = \frac{\ln[1 + \exp(\Delta\sigma J_0 - 1)\exp(-\beta E)]}{\ln[1 + \exp(\Delta\sigma J_0 - 1)]}, \quad (16)$$

where $\beta = (\sigma_1/h\nu)B^{-1}$. The transmission through the sample can be calculated by

$$T(t) = \frac{n(L, t)}{n_0}. \quad (17)$$

Using Eq. (6), we have

$$T(t) = \exp[-\Delta\sigma J_1(L, t)]\exp(-\sigma_2 J_0). \quad (18)$$

Now, using Eq. (14) we obtain

$$T(t) = \frac{\exp(-\sigma_2 J_0)}{1 + \exp(\Delta\sigma J_0 - 1)\exp(-\sigma_1 B^{-1} n_0 t)}. \quad (19)$$

The transmission can also be written as a function of the integrated input energy:

$$T(E) = \frac{\exp(-\sigma_2 J_0)}{1 + \exp(\Delta\sigma J_0 - 1)\exp(-\beta E)}. \quad (20)$$

This can be rewritten as follows:

$$T(E) = \frac{T(\infty)}{1 + [T(\infty)/T(0) - 1]\exp(-\beta E)}, \quad (21)$$

where the initial and final transmissions are

$$T(0) = \exp(-\sigma_1 J_0), \qquad T(\infty) = \exp(-\sigma_2 J_0). \quad (22)$$

B. Numerical Solution

We also obtained numerical solutions to our theoretical model. Unfortunately numerical calculations took too much time to be used routinely to fit our data (B being the fitting parameter): using a numerical solution to fit a plot of 1000 points would take approximately 50 h (with the program written under the Igor Pro application with a Quadra 650 Macintosh). It took only approximately 2 min for the analytical solution. However we have computed numerical solutions for given sets of parameter values in order to compare the approximate analytical solution (used to fit the data) with the exact solution (numerical). With the numerical solution we could also study the influence of different parameters on the evolution of the transmission.

The analytical and numerical solutions were similar even with large values of $\sigma_2 N_0 L$ ($\sigma_2 N_0 L \ll 1$ was the condition for the validity of the approximate analytical solution). Figure 1 shows theoretical plots obtained with the numerical solution and with the approximate analytical solution for $\sigma_2 N_0 L = 0.5$. Thus, the approximate analytical solution can be legitimately used to fit our data provided that $\sigma_2 N_0 L < 0.5$.

The theoretical model offers the possibility to study the influence of different parameters on the evolution of the transmission with time (or the integrated input energy) when photodestruction occurs. Several numerical simulations are plotted in Fig. 2. Each plot shows the evolution of the transmission as a function of the integrated input energy for three different parameters: the concentration of dye molecules [Fig. 2a)], the absorption cross sections σ_1 of the dye molecules and σ_2 of the bleached molecules [Figs. 2b) and 2c)], and the B factor [Fig. 2d)] (average number of photons absorbed by each dye molecule before bleaching). The bold curves in the four panels are plotted with the same set of parameters.

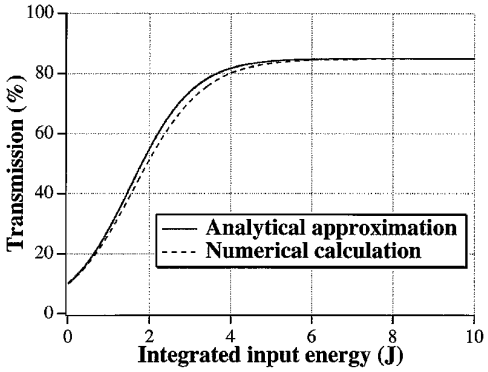

Fig. 1. Comparison of the approximate analytical and exact numerical calculations of the transmission as a function of integrated input energy ($\sigma_2 N_0 L = 0.5$).

The dye concentration affects the initial and final transmissions whereas the rate of photodestruction (i.e., the slope) is not affected [Fig. 2a)]. The absorption cross section σ_1 of the dye molecule affects the initial transmission and the rate of photodestruction whereas the final transmission is not affected [Fig. 2b)]. The absorption cross section σ_2 of the bleached molecule affects just the final transmission [Fig. 2c)]. The B factor affects just the rate of photodestruction [Fig. 2d)].

3. Experimental

A. Sample Preparation

The matrices in which dye molecules were incorporated were made of an inorganic silica network to which vinyl or methyl groups were attached.[1] They were obtained under acid-catalyzed conditions with acetone as the common solvent by hydrolysis condensation of vinyltriethoxysilane or methyltriethoxysilane precursors: $(CH{=}CH_2){-}Si{-}(OC_2H_5)_3$ or $(CH_3){-}Si{-}(OCH_3)_3$. Different dyes such as Perylene Red, Perylene Orange, Pyrromethenes 567 and 597, Rhodamine B, 4-(Dicyanomethylene)-2-methyl-6-(p-dimethylaminostyryl)-4H-pyran (DCM), a Xanthylium salt, and Neon Red were tested as dopants. After gelation, the samples were left to dry for approximately three weeks at 40 °C. Typical dimensions of the samples were approximately 4 cm in diameter and 5 mm thick. Then they were polished to obtain a flatness to within 4 nm. The transmission spectra of the two kinds of undoped matrix are

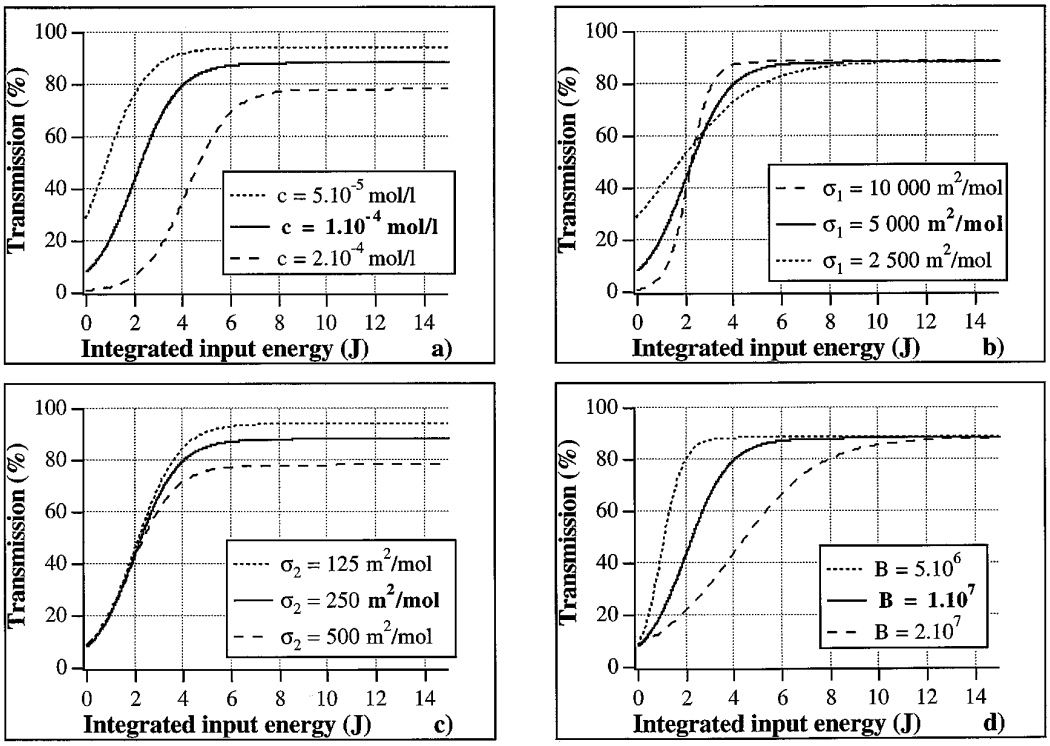

Fig. 2. Simulations of the transmission versus integrated input energy: a) influence of the dye concentration, absorption cross sections of b) the dye molecule and c) the bleached molecule, and d) the B factor (average number of photons absorbed by each molecule before bleaching).

given in Ref. 1. At a wavelength of 532 nm, the index of refraction of the matrices was measured to be 1.5 and the transmission was approximately 92%. Thus, the losses through the matrix itself were due to surface reflection and not to scattering.

We used water and chloroform to perform the experiments with molecules in liquid solutions.

B. Experimental Arrangement

A schematic diagram of the experimental arrangement is shown in Fig. 3. A continuous-wave power-stabilized frequency-doubled linearly polarized Nd:YAG laser provided 40 mW at 532 nm. We were able to attenuate the beam with a combination of neutral density filters. The light was focused into the samples to a spot diameter of 50 μm. The Rayleigh length (10 mm) was twice the typical sample thickness (5 mm) so as to have quasi-plane waves within the sample. The transmitted signal, collected by a lens, passed through another set of neutral density filters and was detected by a power meter that provided voltage to a digital oscilloscope that was connected to a Macintosh. A program using the Igor Pro application was written in order to monitor the evolution of the transmission through the sample as a function of time or as a function of integrated input energy. The curves were divided by the Fresnel factor to compensate the losses that were due to reflection on the surfaces of the samples. Using a reference beam, we were able to correct the fluctuations of the laser power. The experiment was performed at room temperature.

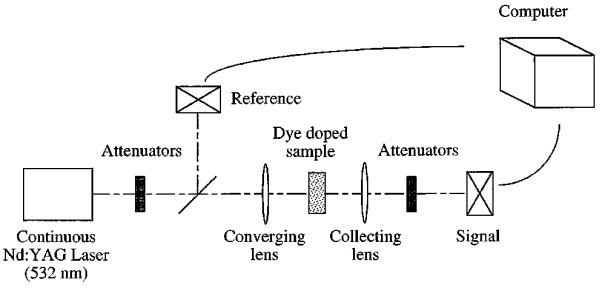

Fig. 3. Experimental setup.

C. Measurements

For each doped solgel sample we made several acquisitions at different input powers. The transmissions were plotted as a function of the integrated input energy. In a one-photon photodestructive process the curves should be similar regardless of the value of the exciting power [Equation (21) in Subsection 2.A]. At high powers we observed that the shape of the curves changed when the power was modified. The experimental protocol was to decrease the input power until the curves no longer changed [Figs. (4a–4c)]. Then the main destructive process was assumed to be a one-photon process ruled by the B factor. Other processes such as multiphoton or thermal processes that obviously occurred at high powers were then neglected. We could then fit the plots with the theoretical model.

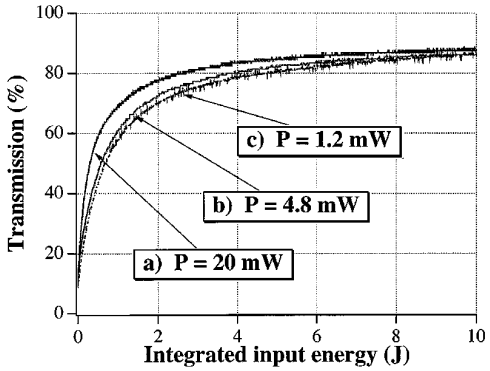

Fig. 4. Evolution of the transmission of a Pyrromethene 567-doped solgel sample versus the integrated input energy for three different power levels.

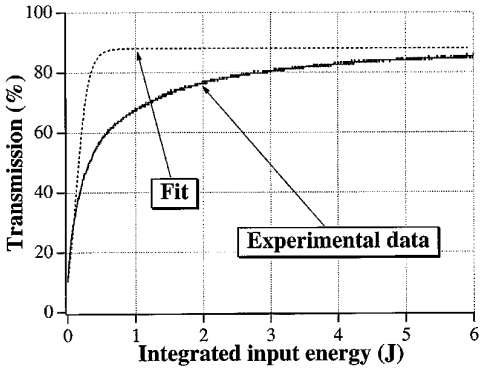

Fig. 5. Fit of the transmission versus integrated input energy for a Pyrromethene 567-doped solgel sample: $B = 2 \times 10^5$.

From the initial and final transmissions we obtained the values of the absorption cross sections σ_1 and σ_2 [see Eq. (22)]. The initial concentration N_0 was chosen so that the initial transmission $T(0)$ was a few percent. Note the condition $\sigma_2 N_0 L \ll 1$, which allows us to use the analytical expression of the transmission to fit our data. With one sample we had $\sigma_1 N_0 L = 0.4$; with the others we had $\sigma_2 N_0 L \ll 1$. The measured values of the initial and final transmissions were taken for the fit. Then the only unknown parameter was the B factor, which was our fitting parameter.

4. Results and Discussion

A. Dyes in Solid Matrices

The model was a good fit with the evolution of the transmission at the beginning but did not fit so well at the end. The difference between the experimental and theoretical results can be explained by the fact that dye molecules are generally not isotropic and their orientation may be fixed[15] by matrix surroundings. If we suppose a random distribution of axial dye molecules fixed in the matrix, the molecules normal to the polarization of incident light are the last to be destroyed. In this case, the curves must be modified because later the sample would contain a larger fraction of molecules with a smaller effective absorption cross section. Using a $\lambda/2$ waveplate, we were able to measure the absorption normal to the incident light polarization at any time during the illumination. The anisotropy parameter r, defined as $r = (A_{\parallel} - A_{\perp})/(A_{\parallel} + 2A_{\perp})$, was calculated for different dyes ($A_{\parallel}$ is the absorption in the direction of the incident light polarization. $A_{\perp}$ is the absorption in the direction normal to the incident light polarization). For example, with a solgel sample doped with Rhodamine B, we measured $r = 0.25$ ($A_{\parallel} = 40\%$, $A_{\perp} = 20\%$) at a transmission of 60% (the transmission started at 1% and finished at 75%); this meant a significant nonisotropic distribution of dye molecules ($r = 0$ in the case of total isotropy when $A_{\parallel} = A_{\perp}$ and $r = 1$ when $A_{\perp} = 0$). Thus, in a more realistic model, the nonisotropic distribution of dye molecules that progressively appear in the matrix during the photodestruction process should be introduced. But then the model would be much more complex and would have only numerical solutions that would preclude the fitting of large amounts of experimental data. Therefore, we chose to fit only the beginning of the plots for which our model was valid because the distribution of dye molecules was then quasi-isotropic. Figure 5 shows the fit of a solgel sample doped with Pyrromethene 567: $B = 2 \times 10^5$. The B factor values were obtained with good precision (approximately $\pm 5\%$) because the quality of the fit was good at the beginning of the plots and the initial slope of the fit depends strongly on the B factor. The B factor values for our dye molecules are reported in Table 1. The most photostable dyes were Perylene Orange and Perylene Red. It is worth noting that they may be quite rapidly destroyed at high flux during thermal processing. This is also the case when we use the samples in pulsed lasers and increase the repetition rate.[2] In addition their efficiency as gain media for pulsed lasers is not the best (40%).[1] We have reported[1] that the stability of Pyrromethene 597 was not affected

Table 1. *B* Factors of Different Doped Solgel Samples and the Corresponding Absorbed Energy[a]

Dye	B	Absorbed Energy (GJ/mol)
Pyrromethene 567	2×10^5	40
	(1.5×10^3)	(0.3)
Pyrromethene 597	2×10^5	40
DCM	6×10^5	120
Neon Red	6.5×10^5	150
Xanthylium salt	1×10^7	2200
Rhodamine 6G	2×10^7	4500
	(3×10^5)	(60)
Rhodamine B	4×10^7	9000
	(5×10^5)	(110)
Rhodamine B (grafted)	8×10^7	18,000
Perylene Red	9×10^8	200,000
Perylene Orange	1×10^9	225,000

[a] B factors correspond to the average number of photons absorbed by a molecule before it is bleached. The values in parentheses represent estimations for the same molecules in solution.

by repetition rate (from 0.2 to 20 Hz) when excited by a pulsed laser, which means that it is less sensitive to thermal effects than Perylene Red but also its photostability is much weaker (by a factor of 4000). We have also reported the stability of Pyrromethene 567 with regard to thermal effects[1] but its photostability is the same as for Pyrromethene 597. Pyrromethenes have high lasing efficiencies in solid matrices (slope efficiencies of approximately 70%.)[1] The much less common dyes, Neon Red and Xanthylium salt, have interesting B values. The famous Rhodamines B and 6G have excellent photostability. However, dyes such as Pyrromethenes 597 and 567 have much higher lasing efficiency (slope efficiency of approximately 40% with Rhodamine B). One can also observe the influence of the matrix with Rhodamine B if it is grafted or not. When grafted, the photostability of Rhodamine B is improved by a factor 2 but its lasing efficiency is reduced by a factor of 6.

To the best of our knowledge, B values for dye molecules such as Perylene Red, Perylene Orange, Pyrromethenes 567 and 597, DCM, a Xanthylium salt, and Neon Red have never been reported. B values of Rhodamine molecules have already been calculated using simpler models neglecting the absorbance of the bleached molecules[9,16,17] (the transmission was assumed to have a final value of 100%). The stability of some of the dye molecules that we investigated has been studied but in different ways. Most recently Rhan and King measured "the accumulated pump energy absorbed by the system per mole of dye molecules in the gain region before the output pulse energy falls to one-half of its initial value."[6] They studied the influence of different solid environments on the stability of trapped dye molecules. Their interesting study shows that stability depends on the environment. However, these measurements were dependent on the samples and the experimental conditions; they were not intrinsic characteristics of the dye molecules. In addition they included all the destructive processes and the samples were used as gain media in a laser system pumped with a pulsed laser. From Eq. (6) in Subsection 2.A, we can give the total input energy $E_{1/2}$ that is necessary to destroy half of the initial dye molecules:

$$E_{1/2} = B\frac{h\nu}{\sigma_1} \times (\Delta\sigma J_0 - 1 - \ln[[1 + \exp(\Delta\sigma J_0 - 1)]^{1/2} - 1]). \quad (23)$$

It is clear that $E_{1/2}$ depends on both the dye molecule and the bleached molecule (B, σ_1, and σ_2) but also on the initial concentration of dye molecules per unit area (J_0). Therefore, $E_{1/2}$ is not intrinsic to the dye molecule. We can calculate the average energy absorbed by a mole of dye molecule by multiplying B by $Nh\nu$ (N is the Avogadro constant). The results

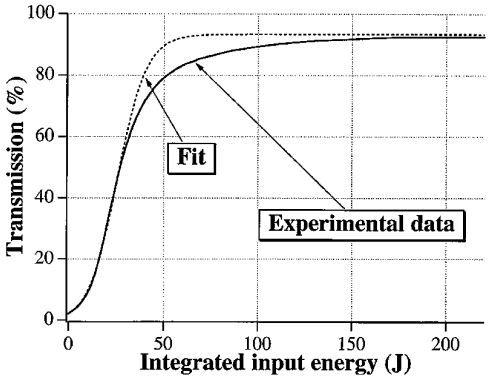

Fig. 6. Fit of the transmission versus integrated input energy for the Pyrromethene 567 dye solution: $B = 1.5 \times 10^3$ (after a volume correction).

are reported in the third column of Table 1. These results are characteristic of the dye molecules but of course, cannot be compared with direct measurements of the absorbed energy that other authors have reported.

B. Dyes in Solutions

The problem of nonisotropic distribution of dye molecules in solid matrices does not exist in solution in which the molecules are free to move. Theoretical curves are then closer to the experimental data in the former case (Fig. 6) than in the latter (Fig. 5). Nevertheless, there is a permanent supply of fresh molecules in the illuminated region where the molecules are bleached. This explains why the experimental transmission does not increase with the integrated input energy (or time) as fast as the calculated transmission especially at the end. This phenomenon of dye replenishment was introduced into the numerical model to fit the data, but the computing time was then much too long. Nevertheless, we used the analytical model with the interactive volume as the total volume of solution and then multiplied the obtained B factor by the ratio of the interactive volume over the total volume.

Three dye molecules were studied in solution: Rhodamine 6G, Rhodamine B, and Pyrromethene 567. We used the same procedures as were used for solgel samples. The estimations of B values are listed in parentheses in Table 1. The photostability of dye molecules trapped in solid matrices was approximately 2 orders of magnitude higher than in solutions. This can be explained by the fact that the dye molecules trapped in the matrices are then partially isolated from reactive impurities such as oxygen, which takes part in the destructive photochemical reactions. Furthermore the rigidity of the matrices and their strong interactions with organic dopants reduce the probability of thermally excited reactions.

5. Conclusions

An experimental study of the photostability of organic dye molecules trapped in solid matrices synthe-

sized by the solgel technique was carried out at room temperature. Using a cw frequency-doubled linearly polarized Nd:YAG laser we observed the coexistence of different destructive effects. At low laser powers we were able to isolate a one-photon photodestructive process. Then we used a theoretical model that we developed in order to match our experimental results. With an approximate analytical solution to the problem for different trapped dye molecules we obtained the average number of photons that were absorbed before bleaching (the B factor). It would be interesting to characterize the slightly absorbing bleached molecules that are progressively created during illumination, which probably explains why the transmission never reaches 100% saturation. To that purpose we expect to perform time-resolved spectra measurements. It would also be interesting to develop a model in which the nonisotropic distribution of dye molecules progressively created in the solgel matrix during the photodestruction process would be taken into account.

We have compared the photostability of different molecules when trapped in solid matrices (Perylenes, Rhodamines, Pyrromethenes). In the same working conditions using the same model, we have shown that the photostability of dye molecules in solid matrices was increased by 2 orders of magnitude compared with molecules in liquid solutions.

References

1. M. Canva, A. Dubois, P. Georges, A. Brun, F. Chaput, A. Ranger, and J. P. Boilot, "Perylene, Pyrromethene and grafted Rhodamine doped xerogels for tunable solid state laser," in *Sol-Gel Optics III,* J. D. Mackenzie, ed., Proc. SPIE **2288,** 298–309 (1994).
2. M. Canva, A. Dubois, P. Georges, A. Brun, F. Chaput, and J. P. Boilot, "Dye doped xerogels for tunable lasers," Adv. Solid-State Lasers **20,** 291–295 (1994).
3. B. Dunn, F. Nishida, R. Toda, J. J. Zink, T. H. Allik, S. Chandra, and J. A. Hutchinson, "Advances in dye-doped sol-gel lasers," Mater. Res. Soc. Symp. Proc. **329,** 267–277 (1994).
4. M. D. Rahn and T. A. King, "Solid state dye doped sol-gel glass composite lasers," in *Conference on Lasers and Electro-Optics,* Vol. 8 of OSA 1994 Technical Digest Series (Optical Society of America, Washington, D.C., 1994), pp. 389–390.
5. R. E. Hermes, T. H. Allik, S. Chandra, and J. A. Hutchinson, "High-efficiency pyrromethene doped solid-state dye lasers," Appl. Phys. Lett. **63,** 877–879 (1993).
6. M. D. Rahn and T. A. King, "Lasers based on doped sol-gel composite glasses," in *Sol-Gel Optics III,* J. D. Mackenzie, ed., Proc. SPIE **2288,** 382–391 (1994).
7. D. Avnir, D. Lévy, and R. Reisfeld, "The nature of the silica cage as reflected by spectral changes and enhanced photostability of trapped Rhodamine 6G," J. Phys. Chem. **88,** 5956–5959 (1984).
8. E. T. Knobbe, B. Dunn, P. D. Fuqua, and F. Nishida, "Laser behavior and photostability characteristics of organic dye doped silicate gel materials," Appl. Opt. **29,** 2729–2733 (1990).
9. I. P. Kaminow, L. W. Stulz, E. A. Chandross, and C. A. Pryde, "Photobleaching of organic laser dyes in solid matrices," Appl. Opt. **11,** 1563–1567 (1972).
10. J. C. Newell, L. Solymar, and A. A. Ward, "Holograms in dichromated gelatin: real-time effects," Appl. Opt. **24,** 4460–4466 (1985).
11. W. J. Tomlinson, E. A. Chandross, R. L. Fork, C. A. Pryde, and A. A. Lamola, "Reversible photodimerization: a new type of photochromism," Appl. Opt. **11,** 533–548 (1972).
12. N. Capolla and R. A. Lessard, "Real time bleaching of methylene blue or thionine sensitized gelatin," Appl. Opt. **30,** 1196–1200 (1991).
13. A. N. Fletcher, "Laser dye stability. Part 4," Appl. Phys. **16,** 93–97 (1978).
14. B. Liphardt, B. Liphardt, and W. Luttke, "Laser dyes III: concepts to increase the photostability of laser dyes," Opt. Commun. **48,** 129–133 (1983).
15. M. Canva, G. Le Saux, P. Georges, A. Brun, F. Chaput, and J. P. Boilot, "All-optical gel memory," Opt. Lett. **17,** 218–220 (1992).
16. D. Beer and J. Weber, "Photobleaching of organic laser dyes," Opt. Commun. **5,** 307–309 (1972).
17. E. P. Ippen, C. V. Shank, and A. Dienes, "Rapid photobleaching of organic laser dyes in continuously operated devices," IEEE J. Quantum Electron. **QE-7,** 178–179 (1971).